

A new Miocene ape and locomotion in the ancestor of great apes and humans

<https://doi.org/10.1038/s41586-019-1731-0>

Received: 10 July 2019

Accepted: 27 September 2019

Published online: 6 November 2019

Madelaine Böhme^{1,2*}, Nikolai Spassov³, Jochen Fuss^{1,2}, Adrian Tröscher², Andrew S. Deane⁴, Jérôme Prieto⁵, Uwe Kirscher^{1,6}, Thomas Lechner^{1,2} & David R. Begun⁷

Many ideas have been proposed to explain the origin of bipedalism in hominins and suspension in great apes (hominids); however, fossil evidence has been lacking. It has been suggested that bipedalism in hominins evolved from an ancestor that was a palmigrade quadruped (which would have moved similarly to living monkeys), or from a more suspensory quadruped (most similar to extant chimpanzees)¹. Here we describe the fossil ape *Danuvius guggenmosi* (from the Allgäu region of Bavaria) for which complete limb bones are preserved, which provides evidence of a newly identified form of positional behaviour—extended limb clambering. The 11.62-million-year-old *Danuvius* is a great ape that is dentally most similar to *Dryopithecus* and other European late Miocene apes. With a broad thorax, long lumbar spine and extended hips and knees, as in bipeds, and elongated and fully extended forelimbs, as in all apes (hominoids), *Danuvius* combines the adaptations of bipeds and suspensory apes, and provides a model for the common ancestor of great apes and humans.

Many studies since the nineteenth century have investigated the origin of human bipedalism. From Darwin and Huxley to the present, many researchers have added insights into this question but with little or no fossil evidence in support^{2–4}. Although many fossils have been discovered, none has shed light directly on this central question in palaeoanthropology.

Since the 1970s, many fossil apes from the middle to late Miocene epoch (13–5.3 million years ago (Ma)) from Europe have been discovered and described, along with smaller samples from the same time period in Africa^{5–7}. Apes and humans are thought to have diverged at this time⁸. Some of these discoveries include partial skeletons^{9,10}, but none shows preservation of completely intact long bones. Although opinions vary as to the relationship of these hominids to living hominids, nearly all researchers recognize European late Miocene apes as hominids as opposed to the stem hominoids of the early and middle Miocene epoch of Africa^{6,11,12}.

Postcranially, the most complete fossils from Europe include the well-preserved remains of the small bones of the hand, fragments of the long bones of the limbs, a partial pelvis and partially preserved vertebrae. These discoveries have provided insights into the anatomy of late Miocene apes. We know that these apes, including *Pierolapithecus*, *Dryopithecus*, *Hispanopithecus* and *Rudapithecus*, were suspensory and similar to modern great apes to varying degrees. However, without complete long bones of the limbs and well-preserved joint surfaces (especially of the lower limbs), interpretations of details of the positional behaviour of these apes remain limited.

Reconstructing the ancestral form of positional behaviour of great apes and humans is best accomplished through the analysis of fossils. On the basis of comparisons of *Ardipithecus*, extant catarrhines and Miocene apes, it has been argued that human bipedalism evolved from a

form of arboreal quadrupedalism in the last common ancestor of great apes and humans^{13,14}. Others have argued that bipedalism arose from a more suspensory ancestor, based largely on fossil evidence of late Miocene hominids^{6,11}. These scenarios are based on fragmentary fossil evidence. Here we present a different scenario based on our analysis of a well-preserved dryopithecine ape from Bavaria. The ulna, femur, tibia, vertebrae, hand and foot bones of this ape reveal unknown aspects of the anatomy of late Miocene apes and enable us to reconstruct what may be the ancestral morphology of the great apes and humans.

Extended limb clambering

The fossils (Fig. 1) include remains of at least four individuals, with a partial skeleton that is sufficiently complete to describe the morphology of the limbs and spine and proportions of the body in detail. The results reveal a combination of anatomical features that are indicative of a pattern of arboreal behaviour that we term extended limb clambering (ELC). It is characterized by generalized limb proportions superimposed on a unique combination of knee, ankle, elbow and wrist postures and strongly grasping extremities. ELC incorporates powerful hallal grasping, plantigrade feet, extended hip and knees, wide ranging elbow flexion–extension and pronation–supination, a mobile wrist, and hands with curved phalanges and a deep first metacarpal joint. It differs from previously identified forms of positional behaviour. Plantigrade and palmigrade quadrupeds (Old World monkeys and *Ekembo*) lack the suspensory attributes of the forelimb and the extension set of the knee. Knuckle-walkers (chimpanzees, bonobos and gorillas) lack the extended knee and have less powerfully developed hallal and pollical grasping. The hand phalanges of *Danuvius* also lack the robusticity typical of

¹Department of Geosciences, Eberhard-Karls-Universität Tübingen, Tübingen, Germany. ²Senckenberg Centre for Human Evolution and Palaeoenvironment, Tübingen, Germany.

³National Museum of Natural History, Bulgarian Academy of Sciences, Sofia, Bulgaria. ⁴Anatomy & Cell Biology, University of Indianapolis, Indianapolis, IN, USA. ⁵Paleontology & Geobiology, Ludwig-Maximilians-Universität, Munich, Germany. ⁶Earth Dynamics Research Group, School of Earth and Planetary Sciences, Curtin University, Perth, Western Australia, Australia.

⁷Department of Anthropology, University of Toronto, Toronto, Ontario, Canada. *e-mail: m.boehme@ifg.uni-tuebingen.de

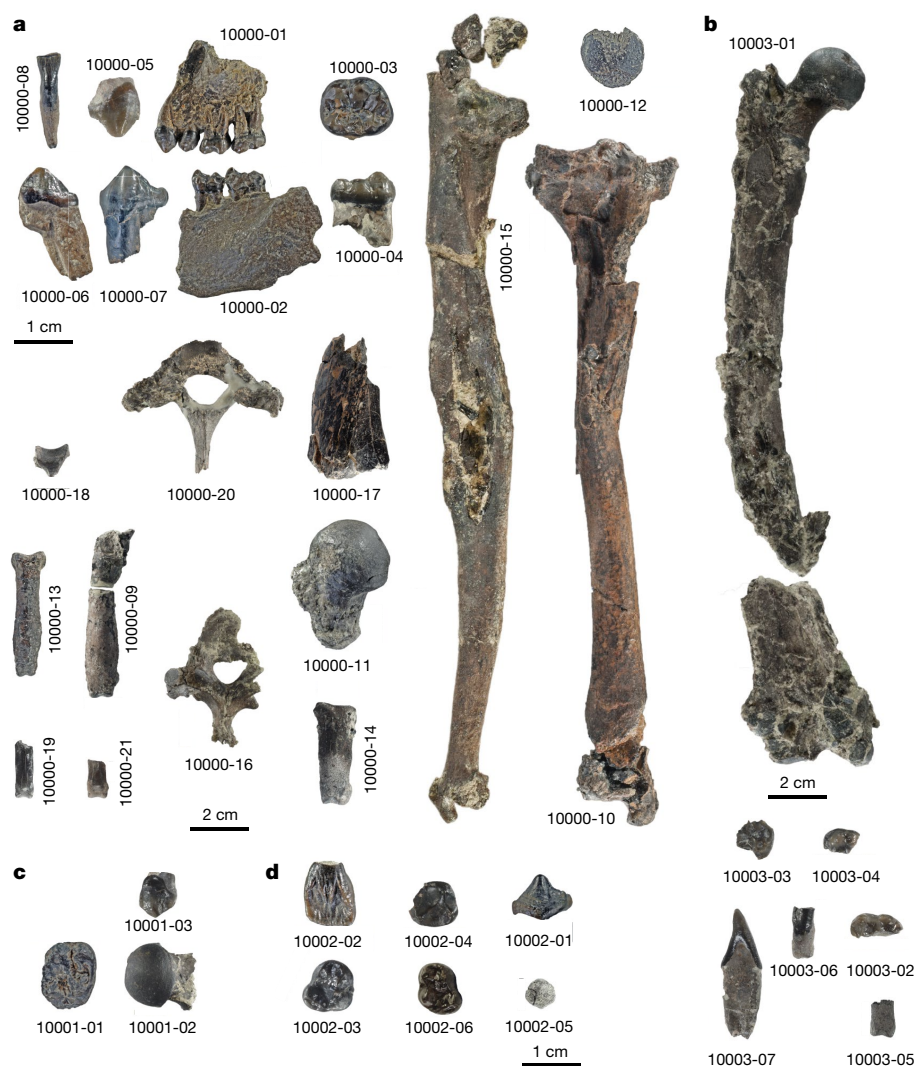


Fig. 1 | Fossil remains of four *D. guggenmosi* individuals from late Miocene sediments of Hammerschmiede. **a**, Holotype GPIT/MA/10000 male individual. **b–d**, Paratype individuals GPIT/MA/10003 (female), GPIT/MA/10001 (female) and GPIT/MA/10002 (juvenile). An excavation plan and a complete list of all elements can be found in Extended Data Fig. 1 and Supplementary Table 2. The scale bar is 20 mm for all bones and 10 mm for all isolated teeth.

knuckle-walkers. Arboreal clambering orangutans lack the weight-bearing adaptations present in the knee and ankle of *Danuvius* and have features that much more strongly emphasize forelimb postural and locomotor adaptations. *Danuvius* is distinguished from all known catarrhines in its vertebral morphology, with an elongated lumbar region combined with spinal invagination/lordosis, which shifts the body mass over the expanded proximal tibial joint surfaces. The uniqueness of ELC is that it does not favour the forelimb or the hindlimb, as in most primates, but utilizes both limbs in roughly equal proportions. ELC includes a combination of joint positions and loading patterns of both hominin bipedalism that emphasize hindlimb extension and spinal curvatures, and extant great ape suspension, which emphasizes powerful and mobile forelimbs. We propose ELC as a new model of the ancestral mode of positional behaviour of the last common ancestor of living great apes and humans. ELC is a precursor to obligate bipedalism, which shifts the emphasis of positional behaviour to the hindlimbs, and to suspension, in which the emphasis shifts to the forelimbs.

Systematic palaeontology

Order Primates Linnaeus, 1758
 Infraorder Catarrhini Geoffroy, 1812
 Family Hominidae Gray, 1825
Danuvius guggenmosi gen. et sp. nov.

Etymology. The genus name is derived from Celtic–Roman river god Danuvius. The trivial name honours the discoverer of the Hammerschmiede locality, Sigulf Guggenmos.

Holotype. Partial skeleton of male individual GPIT/MA/10000, comprising 21 elements (Fig. 1a): partial left mandible with M_1 and M_2 , partial left maxilla with P^3 – M^2 , isolated mandibular (left I_1 , P_3 ; right P_3 , M_2 , M_3) and maxillary teeth (right P^3), first and transitional thoracic vertebrae, left humeral shaft fragment, right ulna, left metacarpal I fragment, right proximal manual phalanges II and IV, two left intermediate manual phalanx fragments, right femoral head, right patella, left tibia, left proximal pedal phalanx I.

Paratypes. Two smaller adults (GPIT/MA/10001 (Fig. 1c), comprising left P^3 , M^1 , left femur head; and GPIT/MA/10003 (Fig. 1b), comprising left I_1 , I_2 , fragments of M_1 , M^1 , M^2 , left femur, proximal hallucal phalanx fragment) and one juvenile individual (GPIT/MA/10002 (Fig. 1d), comprising unerupted left P_3 , left I^1 , left and right DP_4 , right DP^4 , epiphysis of the intermediate manual phalanx).

Locality and horizon. Hammerschmiede Clay pit near Pforzen (Allgäu region, Bavaria, Germany, Extended Data Fig. 1; 47.923° N, 10.588° E); level Hammerschmiede (HAM) 5 at stratigraphic metre 12 in the local section, which has been dated magnetostratigraphically to 11.62 million years ago¹⁵.

Diagnosis. Small hominid ranging in size from about 17 to 31 kg. The palate is narrow and deep with a thick palatine process; the maxilla is high, anteroposteriorly broad, with an anteriorly facing zygomatic root above the distal moiety of P^4 , maxillary sinus invaginating the zygomatic and alveolar processes, canine fossa deep and narrow, canine

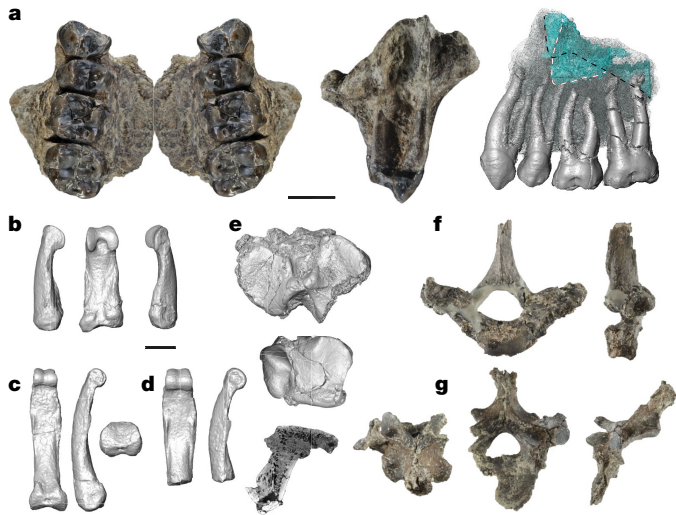


Fig. 2 | *D. guggenmosi* holotype. **a**, Palate (left; right side mirror-imaged) and left maxilla from superior (middle) and lateral (right) views, with a three-dimensional rendering of dental roots and maxillary sinus (blue). The sinus is invaginated by the posterobuccal and lingual roots of M^2 and is superior to the roots more anteriorly (dashed black line). Laterally the sinus extends into the zygomatic root (dashed white line); additional images are shown in Extended Data Fig. 10. **b**, Left proximal hallux phalanx in lateral (left), plantar (middle) and medial (right) views. **c**, Right proximal hand phalanx 2 in palmar (left), ulnar (middle) and proximal (right) views. **d**, Right proximal hand phalanx 4 in plantar (left) and ulnar (right) views. **e**, Tibial proximal (top) and distal (middle) articulations (anterior is up) and sagittal computed tomography cross-section through the middle of the lateral condyle (bottom; superior is up). **f**, First thoracic vertebra in superior (left) and left-lateral (right) views. **g**, Diaphragmatic vertebra in posterior (left), superior (middle) and right-lateral (right) views. Scale bars, 10 mm.

root alveolus vertically oriented; I^1 mesiodistally narrow, high-crowned with a strong lingual pillar and mesial marginal ridge; postcanine dentition with strongly developed crista, P^3 lacks the paraconule, molars are broad relative to the length with compressed trigons and thick enamel; mandibular corpus is low, robust with a prominent mandibular eminence and a broad extramolar sulcus; ulna has a straight shaft, moderately deep proximally, short olecranon, deep, strongly keeled, anteriorly oriented trochlear notch, large, laterally oriented radial notch, large head, short, non-articular styloid process; first metacarpal base strongly dorsopalmarly curved saddle-shaped joint; proximal hand phalanges are long, curved, with strongly developed flexor sheath ridges; femur head projects above the greater trochanter, extension of joint surface onto the superoposterior surface of femoral neck, neck compressed and strongly vertically oriented; tibia with broad proximal end, thickened metaphyses, mediolaterally concave condylar surfaces, lateral condyle anteroposteriorly flat, deeply incised and posteriorly oriented intercondylar notch, prominent intercondylar eminences, trochlear surface roughly square-shaped, strongly keeled, prominent malleolus deeply notched at its base with an anterolaterally expanded joint surface; patella with broad, flat joint surface; proximal hallux phalanx is large, robust at mid shaft, broad proximally, prominent flexor sheath ridges, strong lateral torsion of the distal end; first thoracic vertebra with short, divergent pedicles, strongly divergent zygapophyseal orientations, univertebral rib articulation; penultimate or antepenultimate diaphragmatic vertebra with a prominent metapophysis.

Differential diagnosis. The craniodental morphology of *Danuvius* is diagnostically dryopithecine ('Expanded differential diagnosis of *D. guggenmosi*' in the Methods). The anterior palate (Fig. 2a) is short in comparison with pongines, with a stepped subnasal fossa, as is typical

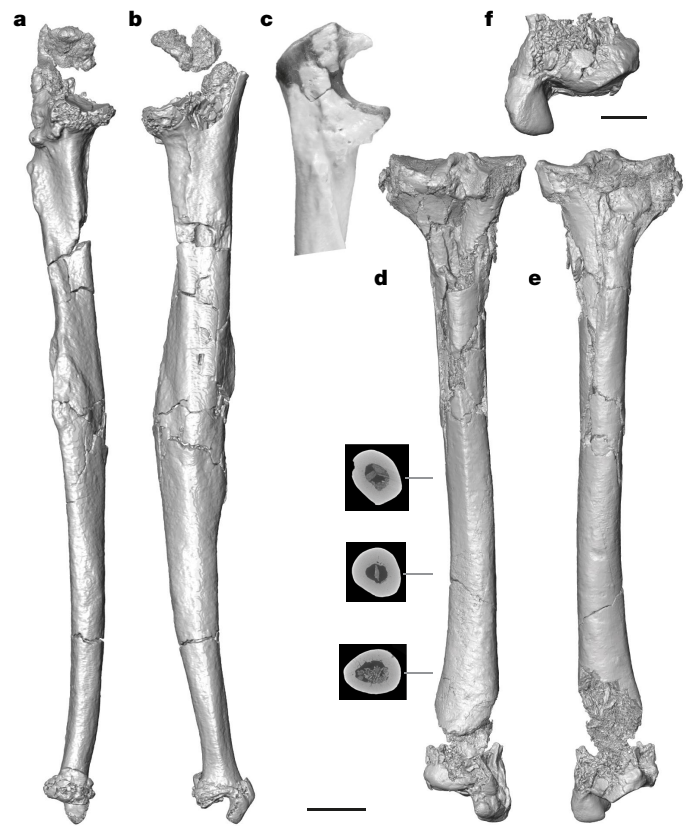


Fig. 3 | *D. guggenmosi*, right ulna (GPIT MA/10000-10) and left tibia (GPIT MA/10000-15). **a–c**, Anterolateral (a) and medial (b) views of the ulna and the reconstructed proximal end in lateral view (c). **d–f**, Posterior (d) and anterior (e) views of the tibia and the distal epiphysis in anterior view (f). Tibial shaft cross-sections are given at 20%, 35% and 50% of shaft length from the distal end. Additional images of the ulna and tibia are shown in Extended Data Fig. 4. Scale bars, 20 mm (a–e) and 10 mm (f).

of dryopithecines and extant hominines. *Danuvius* is distinguished from other dryopithecines in having a unique combination of facial attributes (compressed canine fossa, vertical canine implantation, anteriorly facing malar surface, robust mandible, prominent mandibular eminence, wide extramolar sulcus; Extended Data Fig. 2). The proximal ulna differs from *Hispanopithecus* and *Rudapithecus* in its anteriorly facing trochlear notch and expanded coronoid process (Fig. 3). The distal tibia differs from *Hispanopithecus* in its more squared outline and in details of articular morphology (see Supplementary Information for detailed descriptions and comparisons and Supplementary Tables 3–24 for measurements).

Limb proportions and posture

The postcrania of *Danuvius* reveals numerous previously unknown aspects of dryopithecine morphology. Compared with the length of the tibia, *Danuvius* has a relatively elongated ulna (Fig. 4a and Extended Data Fig. 3), comparable to *Pan paniscus*. In *Pongo*, the ulna is longer whereas in cercopithecoids and early hominins it is shorter. On the basis of reconstructed lengths, *Oreopithecus* and *Hispanopithecus* have tibia:ulna ratios that are comparable to that of *Danuvius*.

A mediolaterally broad thorax and orthograde posture is inferred from the dorsal orientation of the thoracic transverse processes, combined with a low costal facet angle on the first thoracic vertebra¹⁶ (Fig. 2f, g). Inferred from the difference in inclination of the spinous processes between the first vertebra and the lower thoracic vertebra, the upper spinal column was substantially curved (cervical lordosis/thoracic kyphosis)¹⁷.

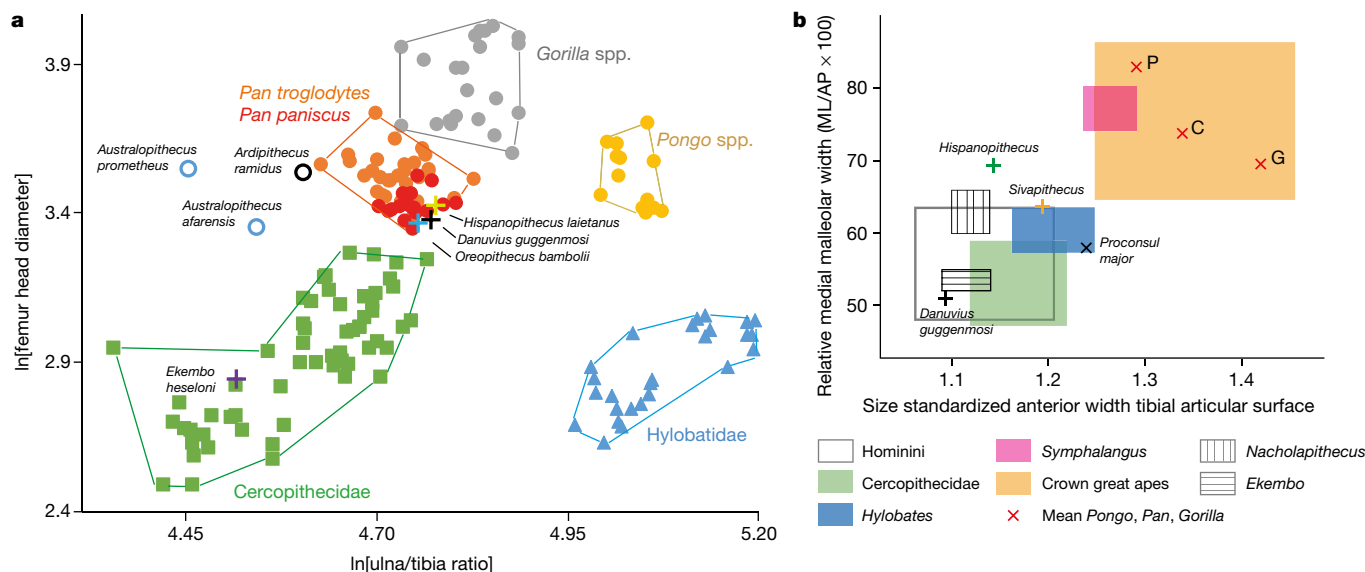


Fig. 4 | Body proportions and distal tibia articulation metrics. a, Ratio of ulna-to-tibia physiologic length (natural logarithm) in relation to body mass (natural logarithm of femur head diameter) of extant catarrhines ($n = 178$; for raw data see Supplementary Table 7) compared to fossil hominoids (*D. guggenmosi*, GPIT/MA10000; *Hispanopithecus laietanus*, IPS 18000; *Oreopithecus bamboli*, IGF 11778; *Ardipithecus ramidus*, ARA-VP-6/500; *Australopithecus prometheus*, StW 573; *Australopithecus afarensis*, A.L. 288-1; *Ekembo heseloni*, KNM-RU 2036; data are from previous studies^{9,13,37–40}). **b**, Plot of relative thickness of tibial

medial malleolus and size-standardized anterior width of tibial distal articular surface (measurements follow a previous study⁴¹) of extant catarrhines, compared to fossil hominoids (*D. guggenmosi*, GPIT/MA/10000; *H. laietanus*, IPS 18000; *Sivapithecus indicus*, YGSP 1656; *Nacholapithecus kerioi*, KNM-BG 35250; *E. heseloni*, KNM-RU 2036, 3589; *Proconsul major*, NAPI 58; comparative data were obtained from previous studies^{31,32,41}; for raw data see Supplementary Tables 19, 20). C, *Pan*; G, *Gorilla*; P, *Pongo*.

D. guggenmosi is, to our knowledge, the first Miocene hominid with evidence of diaphragmatic vertebra placement, which is important in interpreting thoracolumbar spine evolution in hominoids¹⁸. The well-developed costotransversal facet of GPIT/MA/10000-16 (Fig. 2g) indicates a non-ultimate thoracic position for the diaphragmatic vertebra and therefore a functionally longer lower back, as in early hominins, stem-hominoids and cercopithecids^{18–24}. On the basis of indirect evidence from the pelvis, a longer lower back has also been inferred for *Rudapithecus*²⁵. Extant hominoids including *Homo* show a diaphragmatic placement at the ultimate thoracic vertebra level²⁴. The contrasting vertebral configuration of *Danuivius* suggests that diaphragmatic cranial displacement is the symplesiomorphic hominoid condition, supporting the long-back model^{26,27}. The increased number of functional lumbar vertebrae allows sagittal flexibility to lordose the lumbar column, which contributes to effectively position the centre of mass over extended hips, knees and plantigrade feet (see below), implying at least some degree of habitual bipedal posture¹⁶.

Positional behaviour

Several skeletal elements of the upper limb bear unmistakable hallmarks of below-branch or suspensory positional behaviour (Fig. 3a–c and Extended Data Fig. 4). Despite the pathology evident on the ulna (Supplementary Information), these include a reduced olecranon process, broad, keeled trochlear notch with prominent medial and lateral surfaces for a trochlear humeral trochlea, large laterally oriented radial facet, robust proximal ulnar shaft and a reduced, non-articular ulnar styloid process. The proximal hand phalanges are curved with prominent flexor sheath ridges (Fig. 2c, d and Extended Data Figs. 5, 6), indicating that suspension played an important—but not dominant—part in its locomotory repertoire (for example, more similar to *Pan* than to *Pongo*). Powerful pollical grasping and increased thumb mobility are indicated by the strong dorsopalmar and radioulnar curvatures of the base of the first metacarpal (Fig. 1a).

The lower limb suggests postural extension at the hip and knee joints and a uniform force distribution in a stabilized ankle joint, combined with a powerful grasping hallux. On the femur (Fig. 1b and Extended

Data Fig. 7b–d), the low greater trochanter, the more vertically oriented neck and the posterosuperior expanded joint surface suggest that the femoral head articulated in habitual extension with an os coxae that was laterally rotated, which would have caused the iliac blade to be more tilted inferolaterally. This may have enhanced the function of the gluteal muscles as hip stabilizers (abductors) in bipedal posture, as in hominins. The flat patella (Fig. 1a and Extended Data Fig. 7a) and shallow rounded patellar surface suggest slow and deliberate movements (Supplementary Information). The absence of an anteroposterior convexity to the lateral tibial condyle (Fig. 2e and Extended Data Fig. 8), a character shared with hominins and hylobatids²⁸, suggests an extension set to the knee joint, as a flatter contour maximizes tibiofemoral contact area and joint stability during extended knee postures. A buttressing of the tibial metaphysis also reflects stereotypical extended knee postures under compressive load^{28,29}. The exceptional development of the intercondylar eminence is probably related to the presence of strongly developed cruciate ligaments. The subequal size of the tibial condyles indicate a more equally distributed weight transmission on the knee joint³⁰. Together, the morphology of the tibial plateau suggests an adaptation emphasizing an extended knee reinforced by strongly developed intra-articular ligaments. We interpret the distal tibia of *Danuivius*, with its mediolaterally short anterior trochlear margin and its mediolaterally narrow malleolus (Fig. 4b), to be an adaptation to a more uniform distribution of forces across the joint surface, with limited ankle loading in dorsiflexion and inversion compared to extant apes^{31,32}. The combination of the anteroposteriorly deep malleolus, medially expanded joint surface, prominent anterior margin with a strongly developed beak and strongly inclined medial and lateral trochlear surfaces produces a hinge-like morphology to the anterior talocrural joint, which would have been most stable with the foot roughly perpendicular to the long axis of the tibia. This is corroborated by the nearly perpendicularly orientated tibia relative to the horizontal plane of the ankle joint (Fig. 3d, e and Supplementary Information). Extant great apes, which load the ankle in inversion during climbing, have an obliquely oriented tibia relative to the plane of the ankle joint^{31,33}. The near perpendicular tibial angle is a shared

character between hominins and *Danuvius* and supports the inference of a habitual valgus knee position and bipedalism for the new genus.

A robust, elongated and strongly laterally torsioned hallux (Extended Data Figs. 5b, c, 9) with well-developed muscular attachments suggests an emphasis on powerful hallucal grasping with adducted ankle stabilized in a neutral position relative to the long axis of the tibia. In contrast to extant apes, the hallux was capable of interphalangeal hyperflexion, as indicated by the substantial plantar inter-condylar recess and depression (Fig. 2b), enabling *Danuvius* to securely grasp small-diameter arboreal supports.

Discussion

The uniqueness of *D. guggenmosi* is demonstrated by its small body size (between siamangs and bonobos; Supplementary Information and Supplementary Table 23) with limb proportions most similar to bonobos (Fig. 4a), a cranial shifted diaphragmatic vertebra (Fig. 2g), a strong grasping hallux (Fig. 2b) and a morphology of the tibia that is surprisingly similar to hominins (large-sized and flat lateral condyle with 'buttressed' plateau, tibial shaft perpendicular to talar facet, mediolaterally narrow malleolus and short anterior trochlear margin) (Fig. 3d–f, Extended Data Fig. 4 and Supplementary Information). The combination of morphological attributes of the limbs and vertebra of *Danuvius* point to a newly recognized form of positional behaviour. In contrast to suspensory behaviour, clambering and arm-assisted bipedalism in *Pongo*³⁴ or climbing and suspension in African apes, ELC involves equal contributions of the fore- and hindlimbs. The foot is flat and adducted on horizontal to mildly inclined branches with a hallux capable of powerful grasping, stabilizing the hindlimb. Torques resulting from body rotation above the knee are countered by powerfully developed cruciate ligaments. The knee is habitually extended and supported by a thickened plateau and large, flat-to-concave, proximally facing condyles. The elbow is capable of a full range of flexion–extension and pronation–supination as in extant hominoids. The hand was strong enough to generate the force to counter torques in a variety of positions ranging from suspensory to palmigrade, but without the hyperextension at the metacarpophalangeal joints that characterize Old World monkeys and *Pierolapithecus*. This newly defined locomotor category includes attributes of orthograde suspension and hominin bipedalism, making it a potential candidate for the positional behaviour of the last common ancestor of great apes and humans. *Danuvius* provides fossil evidence that hominin bipedalism and great ape suspension evolved from a form of arboreal locomotion that incorporates attributes of each^{35,36}, which has roots in the middle Miocene of Europe.

Online content

Any methods, additional references, Nature Research reporting summaries, source data, extended data, supplementary information, acknowledgements, peer review information; details of author contributions and competing interests; and statements of data and code availability are available at <https://doi.org/10.1038/s41586-019-1731-0>.

1. Begun, D. R. in *Biped to Strider: The Emergence of Modern Human Walking* (eds Meldrum, D. J. & Hilton, C. E.) 9–33 (Kluwer, 2004).
2. Begun, D. R. & Kivell, T. L. Knuckle-walking in *Sivapithecus*? The combined effects of homology and homoplasy with possible implications for pongine dispersals. *J. Hum. Evol.* **60**, 158–170 (2011).
3. Richmond, B. G., Begun, D. R. & Strait, D. S. Origin of human bipedalism: the knuckle-walking hypothesis revisited. *Am. J. Phys. Anthropol.* **116**, 70–105 (2001).
4. Crompton, R. H., Sellers, W. I. & Thorpe, S. K. Arboreality, terrestriality and bipedalism. *Phil. Trans. R. Soc. Lond. B* **365**, 3301–3314 (2010).
5. Begun, D. R. Dryopithecines, Darwin, de Bonis, and the European origin of the African apes and human clade. *Geodiversitas* **31**, 789–816 (2009).
6. Begun, D. R., Nargolwalla, M. C. & Kordos, L. European Miocene hominids and the origin of the African ape and human clade. *Evol. Anthropol.* **21**, 10–23 (2012).
7. Alba, D. M. Fossil apes from the valles-penedès basin. *Evol. Anthropol.* **21**, 254–269 (2012).
8. Langergraber, K. E. et al. Generation times in wild chimpanzees and gorillas suggest earlier divergence times in great ape and human evolution. *Proc. Natl Acad. Sci. USA* **109**, 15716–15721 (2012).

9. Moyà-Solà, S. & Köhler, M. A *Dryopithecus* skeleton and the origins of great-ape locomotion. *Nature* **379**, 156–159 (1996).
10. Moyà-Solà, S., Köhler, M., Alba, D. M., Casanovas-Vilar, I. & Galindo, J. *Pierolapithecus catalaunicus*, a new Middle Miocene great ape from Spain. *Science* **306**, 1339–1344 (2004).
11. Alba, D. M., Almécija, S., Casanovas-Vilar, I., Méndez, J. M. & Moyà-Solà, S. A partial skeleton of the fossil great ape *Hispanopithecus laietanus* from Can Feu and the mosaic evolution of crown-hominoid positional behaviors. *PLoS ONE* **7**, e39617 (2012).
12. Begun, D. R. in *Handbook of Paleoanthropology* (eds Henke, W. & Tattersall, I.) 1261–1332 (Springer, 2015).
13. Lovejoy, C. O., Suwa, G., Simpson, S. W., Matternes, J. H. & White, T. D. The great divides: *Ardipithecus ramidus* reveals the postcrania of our last common ancestors with African apes. *Science* **326**, 73–106 (2009).
14. White, T. D., Lovejoy, C. O., Asfaw, B., Carlson, J. P. & Suwa, G. Neither chimpanzee nor human, *Ardipithecus* reveals the surprising ancestry of both. *Proc. Natl Acad. Sci. USA* **112**, 4877–4884 (2015).
15. Kirscher, U. et al. A biochronologic tie-point for the base of the Tortonian stage in European terrestrial settings: magnetostratigraphy of the topmost Upper Freshwater Molasse sediments of the North Alpine Foreland Basin in Bavaria (Germany). *Newsl. Stratigr.* **49**, 445–467 (2016).
16. Williams, S. A. & Russo, G. A. Evolution of the hominoid vertebral column: the long and the short of it. *Evol. Anthropol.* **24**, 15–32 (2015).
17. Latimer, B. & Ward, C. V. in *The Nariokotome Homo erectus Skeleton* (eds Walker, A. & Leakey, R.) 266–293 (Springer, 1993).
18. Williams, S. A., Middleton, E. R., Villamil, C. I. & Shattuck, M. R. Vertebral numbers and human evolution. *Am. J. Phys. Anthropol.* **159**, 19–36 (2016).
19. Haeusler, M., Regula, S. & Thomas, B. Modern or distinct axial bauplan in early hominins? A reply to Williams (2012). *J. Hum. Evol.* **63**, 557–559 (2012).
20. Nakatsukasa, M. & Kunimatsu, Y. *Nacholapithecus* and its importance for understanding hominoid evolution. *Evol. Anthropol.* **18**, 103–119 (2009).
21. Pilbeam, D. The anthropoid postcranial axial skeleton: comments on development, variation, and evolution. *J. Exp. Zool.* **302B**, 241–267 (2004).
22. Ward, C. V., Walker, A., Teaford, M. F. & Odhiambo, I. Partial skeleton of *Proconsul nyanzae* from Mfangano island, Kenya. *Am. J. Phys. Anthropol.* **90**, 77–111 (1993).
23. Ward, C. V., Nalley, T. K., Spoor, F., Tafforeau, P. & Alemseged, Z. Thoracic vertebral count and thoracolumbar transition in *Australopithecus afarensis*. *Proc. Natl Acad. Sci. USA* **114**, 6000–6004 (2017).
24. Williams, S. A. Placement of the diaphragmatic vertebra in catarrhines: implications for the evolution of dorsostability in hominoids and bipedalism in hominins. *Am. J. Phys. Anthropol.* **148**, 111–122 (2012).
25. Ward, C. V., Hammond, A. S., Plavcan, J. M. & Begone D. R. A late Miocene hominid partial pelvis from Hungary. *J. Hum. Evol.* <https://doi.org/10.1016/j.jhevol.2019.102645> (2019).
26. McCollum, M. A., Rosenman, B. A., Suwa, G., Meindl, R. S. & Lovejoy, C. O. The vertebral formula of the last common ancestor of African apes and humans. *J. Exp. Zool.* **314B**, 123–134 (2010).
27. Lovejoy, C. O. & McCollum, M. A. Spinopelvic pathways to bipedality: why no hominids ever relied on a bent-hip–bent-knee gait. *Phil. Trans. R. Soc. Lond. B* **365**, 3289–3299 (2010).
28. Landis, E. K. & Karnick, P. A three-dimensional analysis of the geometry and curvature of the proximal tibial articular surface of hominoids. In *Proc. SPIE 60560K Three-Dimensional Image Capture and Applications VII 60560K* (International Society for Optics and Photonics, 2006).
29. Frelat, M. A. et al. Evolution of the hominin knee and ankle. *J. Hum. Evol.* **108**, 147–160 (2017).
30. Tardieu, C. Ontogeny and phylogeny of femoro-tibial characters in humans and hominid fossils: functional influence and genetic determinism. *Am. J. Phys. Anthropol.* **110**, 365–377 (1999).
31. DeSilva, J. M. Functional morphology of the ankle and the likelihood of climbing in early hominins. *Proc. Natl Acad. Sci. USA* **106**, 6567–6572 (2009).
32. DeSilva, J. M., Morgan, M. E., Barry, J. C. & Pilbeam, D. A hominoid distal tibia from the Miocene of Pakistan. *J. Hum. Evol.* **58**, 147–154 (2010).
33. Latimer, B., Ohman, J. C. & Lovejoy, C. O. Talocrural joint in African hominoids: implications for *Australopithecus afarensis*. *Am. J. Phys. Anthropol.* **74**, 155–175 (1987).
34. Thorpe, S. K., Holder, R. L. & Crompton, R. H. Origin of human bipedalism as an adaptation for locomotion on flexible branches. *Science* **316**, 1328–1331 (2007).
35. Thorpe, S. K., McClymont, J. M. & Crompton, R. H. The arboreal origins of human bipedalism. *Antiquity* **88**, 906–914 (2014).
36. Wolpoff, M. *Australopithecus*: a new look at an old ancestor (part 2). *Gen. Anthropol.* **3**, 1–5 (1997).
37. Straus, W. in *Classification and Human Evolution* (ed. Washburn, S. L.) 146–177 (Aldine, 1963).
38. Asfaw, B. et al. *Australopithecus garhi*: a new species of early hominid from Ethiopia. *Science* **284**, 629–635 (1999).
39. Ruff, C. B. Long bone articular and diaphyseal structure in Old World monkeys and apes. II: estimation of body mass. *Am. J. Phys. Anthropol.* **120**, 16–37 (2003).
40. Haile-Selassie, Y. et al. An early *Australopithecus afarensis* postcranium from Woranso-Mille, Ethiopia. *Proc. Natl Acad. Sci. USA* **107**, 12121–12126 (2010).
41. DeSilva, J. M. *Vertical Climbing Adaptations in the Anthropoid Ankle and Midfoot: Implications for Locomotion in Miocene Catarrhines and Plio-Pleistocene Hominins*. PhD thesis, Univ. Michigan, (2008).

Publisher's note Springer Nature remains neutral with regard to jurisdictional claims in published maps and institutional affiliations.

© The Author(s), under exclusive licence to Springer Nature Limited 2019

Methods

Geology, age, fossils and taphonomy

The HAM 5 channel represents a riffle pool sequence of a small and shallow meandering rivulet with a talweg width of 4–5 m and a maximum pool depth of 1 m. The gravelly bed load is composed exclusively of reworked pedogenic carbonate concretions that are typically 4–8 mm in diameter. Similar concretions are abundant in Bk palaeosol horizons of the bedrock, indicating a local source of HAM 5 rivulet. Magnetostratigraphy of the local 26-m thick section, combined with a nearby 150 m deep drill core, revealed the date of the channel fill of 11.620 million years ago (± 5 thousand years), directly at the base of the Tortonian, late Miocene¹⁵. Excavation of about 200 m² between 2011 and 2018 revealed a high vertebrate diversity that comprised 100 species of fishes, amphibians, reptiles, birds and mammals (see Supplementary Table 1 for faunal list). Hominids are a common element in this thanatocoenosis, representing about 10% of all excavated large mammal individuals. Excavation demonstrates that fossil vertebrates are found exclusively along the channel, suggesting some sort of accumulation. Most finds are disarticulated skeletal elements, which tend to be complete in small- and medium-sized mammals (for example, carnivores, artiodactyls and primates) and broken and sometimes abraded in large-size taxa (for example, perissodactyls and proboscideans). Skeletal articulation occurs in rare cases. However, many medium-sized individuals are documented by associated specimens found within a few square metres, suggesting minor transport and sorting of bones. The 21 bones and teeth from the most complete hominid individual GPIT/MA/10000 represent about 15% of the skeleton. It is found within the talweg at a maximum distance of 20 m, except the first thoracic vertebra, which was found a further 10 m downstream. Moderate sorting of GPIT/MA/10000 is documented by proximal concentration of isolated teeth, followed by skull elements and more distally long bones and phalanges, whereas vertebrae are transported furthest down the channel (Extended Data Fig. 1). This arrangement follows experimentally observed patterns of bone taphocoenosis in rivers⁴².

Fossil repository

All Hammerschmiede fossils are stored in the palaeontological collection of the University of Tübingen (acronym GPIT), a research infrastructure of the Senckenberg Institute for Human Evolution and Palaeoenvironment (SHEP) Tübingen.

Bone preservation

The Hammerschmiede locality is an active clay-mining pit. Sediments from the fossiliferous rivulet channel HAM 5 are composed of fine-pebbly pedogenic carbonate nodules and marls with various degrees of silt and rare fine-sand admixture. Owing to mining activities, water-saturated clay-rich sediments on steep section walls tend to creep and heavy machinery add compressive load on the sediment surface. Therefore, postcranial long bones of smaller large mammals (for example, deer, tragulids, carnivores and primates) tend to be compressed at the shaft and occasionally laterally distorted. This strongly affected the complete femur of GPIT/MA/10003 (shaft compressed by machinery loading, folded along the shaft due to ground creeping), which was embedded in soft clay. The complete ulna of GPIT/MA/10000 is uncompressed, but at midshaft the cortical bone of the down-lying side is crushed and pushed into the shaft, probably by load compression. Computer tomographic images show that this preservation was facilitated by midshaft osteoporosis. By contrast, the complete tibia of GPIT/MA/10000, embedded in a less compressible silt-dominated matrix, is not crushed along the shaft, but laterally distorted at the tuberosity and slightly damaged at medial condyle and distal metaphysis, which are the result of excavation artefacts. Importantly, all cranial and small postcranial ape specimens (phalanges, metapodial, carpal bone and patella), as well as long-bone joint

articulations remained undisturbed, but occasionally show small excavation artefacts.

Length reconstruction

To measure the total and physiologic length of distorted long bones, we use three-dimensional prints of virtual reconstructions for the holotype tibia and ulna (GPIT/MA/10000-10 and -15, respectively). The total length of the crushed paratype femur (GPIT/MA/10003-01) is estimated with an accuracy of about ± 5 mm.

Expanded differential diagnosis of *D. guggenmosi*

The molars lack cingula and are elongated relative to length, with peripheralized cusps. These attributes and P₃ cusp morphology, P₄ length and M₁–M₂ proportions distinguish *Danuvius* from *Ekembo* and other early Miocene hominoids. The dentition is readily distinguished from thickly enamelled middle and late Miocene apes such as *Kenyapithecus*, *Nacholapithecus*, *Griphopithecus*, *Sivapithecus* and *Ouranopithecus*.

The maxilla of *D. guggenmosi* (Figs. 1a, 2a and Extended Data Figs. 2a, 3a) differs from *Anoiapithecus*, *Pierolapithecus* and *Dryopithecus* in its anteroposteriorly broad zygomatic root (zygomatico-alveolar crest) and convex and postero-inferiorly inclined temporal surface; deeply invaginated maxillary sinus floor; vertically implanted upper male canine (supero-inferiorly and mediolaterally); deep, anteroposteriorly narrow canine fossa and anteriorly facing zygoma. Differs from *Hispanopithecus* and *Rudapithecus* maxilla in its deep, anteroposteriorly narrow canine fossa and anteriorly facing zygoma, anteriorly positioned zygomaticoalveolar crest and deeper palate. Maxillary dentition differs from *Anoiapithecus*, *Pierolapithecus* and *Dryopithecus* by broader premolars; triangular P³; low mesial and distal P³ buccal shoulders; more mesiodistally centralized premolar cusps (shorter talon); broad, concave premolar trigon and talon basins; more strongly developed molar crista; more peripheralized cusps; mesiodistally compressed trigon. I¹ differs from *Pierolapithecus* and cf. *Dryopithecus* sp. (La Grive) in its more strongly developed mesial marginal ridge and convex lingual surface. The maxillary dentition differs from *Hispanopithecus* and *Rudapithecus* in its low P³ crown shoulders and broad upper premolars. The mandible (Fig. 1a and Extended Data Fig. 2b) differs from *Anoiapithecus* and *Dryopithecus* in its shallower, robust corpus (unknown in *Pierolapithecus*), prominent mandibular eminence and wide extramolar sulcus. Mandibular dentition differs from *Anoiapithecus* and *Dryopithecus* in its lower crowned, mesially more vertical P₃ with a prominent mesial beak; broader molar trigonid and talonid basins; shorter mesial fovea; absence of buccal cingula; elongated molars; short M₁ roots (not visible in *Anoiapithecus*). The mandible differs from *Hispanopithecus* and *Rudapithecus* mandibles in the same way as from *Anoiapithecus*, *Pierolapithecus* and *Dryopithecus* and from the lower teeth of *Hispanopithecus* and *Rudapithecus* in having restricted mesial and distal fovea. The mandibular dentition differs from *Ouranopithecus* as it is smaller with more thinly enamelled teeth and it differs in other attributes as in *Rudapithecus* and *Hispanopithecus*. It also differs from *Oreopithecus* in having lower postcanine cusps, less strongly developed crista/cristids, no centroconid, higher P₄ talonid, higher crowned I¹, no upper postcanine lingual cingula. The maxilla differs from early and middle Miocene hominoids in the high position of the zygomatic root. The dentition differs from early and middle Miocene hominoids in the absence of molar cingula, first and second molars of similar size, peripheralized molar cusps, more vertical mesiobuccal P³ surface and short P⁴ shoulders, and higher P₄ talonid.

The partial skeleton GPIT/MA/10000 includes dental and postcranial remains that are much larger than the other Hammerschmiede individuals. This along with the strongly flared mesiobuccal face of the P₃ (Fig. 1a and Extended Data Fig. 2g, j) and the large, elongated canine alveolus (Fig. 2a) strongly imply that GPIT/MA 10000 is a male.

Body mass calculations

For the calculation of the body mass of the individuals, we used metric traits (individual measurements) from hind limbs (femur and tibia) because they are most involved in weight carrying during locomotion in great apes³⁹. Our univariate body-mass predictions are based on regression equations from a previously published study³⁹ for sex/species means of hominoids. In addition, as we can show that body proportions of the male individual GPIT/MA/10000 fall within the range of bonobos and chimpanzees, we assume a comparable scaling pattern and apply regression equations established previously⁴³ for femur head size of the genus *Pan*. Both methods produce very similar results for the male individual within the 50% confidence interval (Supplementary Table 23). Femur size of the two female specimens GPIT/MA/10001 and GPIT/MA/10003 are significantly lower than of any extant great ape, and hence outside any hominid comparative sample. We therefore use the previously compiled regression equations³⁹ for the total primate sample (hominoids plus cercopithecoids) for the predictor femur head size and cercopithecoid equations for predictions based on femoral condyle breadth (as recommended in the previously published study³⁹).

Calculations of enamel thickness

We used the right M₂ of the holotype (GPIT/MA/10000-03) to calculate enamel thickness given its low occlusal wear (slightly higher on mesial half, wear stage 1–2 according to a previously published study⁴⁴). This tooth was scanned with a FF35 CT at the YXLON Application centre in Heilbronn (Germany) and captured at 170 kV and 55 μ A (500-ms exposure time), obtaining a voxel size of 15.8 μ m (Extended Data Fig. 3b). Following a previously published study⁴⁵, virtual buccolingual sections of the molar were performed using Avizo 9.0. Mesial and distal virtual sections were defined by the tips of the metaconid–protoconid and entoconid–hypoconid perpendicular to the cervical plane. The following variables were measured two-dimensionally in both planes: dentine area (*b*), enamel cap area (*c*), length of the enamel–dentine junction (*e*) and the bi-cervical diameter. The average enamel thickness was calculated as *c/e* and the relative enamel thickness (RET) was calculated as previously described⁴⁶ using $RET = 100 \times \left[\frac{(c/e)}{\sqrt{b}} \right]$. For GPIT/MA/10000-03, the RET = 19.36, based on data from the least worn distal section (Supplementary Table 6).

Ellipse estimates of lateral tibial condyle curvature

To estimate the shape of the lateral tibial condyle, we performed a cut through the sagittal mid-line of the condyle on the three-dimensional scans of tibiae from *D. guggenmosi* (Fig. 2e) and extant catarrhines (Extended Data Fig. 6) using an Artec Space Spider with Artec Studio 11 (three-dimensional scans) and Avizo 9 (cross-sections). Subsequently, the cross-sections were digitalized and a best-fit ellipse was obtained using a non-iterative MATLAB function ('EllipseDirectFit'; from

N. Chernov (code available from <https://www.mathworks.com/>)). To compare the individual ellipses, we further calculated the eccentricity $e = \sqrt{1 - (b/a)^2}$ in which *a* and *b* are the semi-major and semi-minor axes with $a \geq b$. The closer *e* is to 1, the more elongated the ellipse is, whereas $e = 0$ represents a circle.

Reporting summary

Further information on research design is available in the Nature Research Reporting Summary linked to this paper.

Data availability

All data generated or analysed during this study are included in this published Article (and its Supplementary Information). The computed tomography scans are available from the corresponding author on reasonable request. The new taxon has the following Life Science Identifier: <http://zoobank.org/References/E1573024-9543-4B1E-A79B-6E40896A4617>.

- Behrensmeyer, A. K. The taphonomy and paleoecology of Plio-Pleistocene vertebrate assemblages east of Lake Rudolf, Kenya. *Bull. Mus. Comp. Zool.* **146**, 473–578 (1975).
- Almécija, S. et al. The femur of *Orrorin tugenensis* exhibits morphometric affinities with both Miocene apes and later hominins. *Nat. Commun.* **4**, 2888 (2013).
- Smith, B. H. Patterns of molar wear in hunger-gatherers and agriculturalists. *Am. J. Phys. Anthropol.* **63**, 39–56 (1984).
- Smith, T. M., Olejniczak, A. J., Martin, L. B. & Reid, D. J. Variation in hominoid molar enamel thickness. *J. Hum. Evol.* **48**, 575–592 (2005).
- Martin, L. B. *The Relationships of the later Miocene Hominoidea*. PhD thesis, Univ. College London (1983).
- Wessel, P. et al. Generic mapping tools: improved version released. *EOS* **94**, 409–410 (2013).
- Amante, C. & Eakins, B. W. *ETOPO11 Arc-Minute Global Relief Model: Procedures, Data Sources and Analysis NOAA Technical Memorandum NESDIS NGDC-24* <https://www.ngdc.noaa.gov/mgg/global/relief/ETOPO1/docs/ETOPO1.pdf> (National Geophysical Data Center, NOAA, 2009).
- Reuter H. I., Nelson, A. & Jarvis, A. An evaluation of void-filling interpolation methods for SRTM data. *Int. J. Geogr. Inf. Sci.* **21**, 983–1008 (2007).
- Almécija, S., Alba, D. M. & Moyà-Solà, S. *Pierolapithecus* and the functional morphology of Miocene ape hand phalanges: paleobiological and evolutionary implications. *J. Hum. Evol.* **57**, 284–297 (2009).

Acknowledgements We are indebted to the following researchers and curators for granting access to collections under their care: S. Moyà-Solà and D. Alba, E. Gilissen, L. Costeur, A. van Heteren, S. Merker, E. Weber. We thank C. Schulbert and J.-F. Metayer for computed tomography scanning, and A. Fatz, H. Stöhr and W. Gerber for technical support.

Author contributions M.B. and D.R.B. designed the study; M.B., N.S., J.F., A.T., A.S.D., J.P., U.K., T.L. and D.R.B. collected the data and performed the analyses; M.B., D.R.B. and N.S. discussed the results and wrote the paper.

Competing interests The authors declare no competing interests.

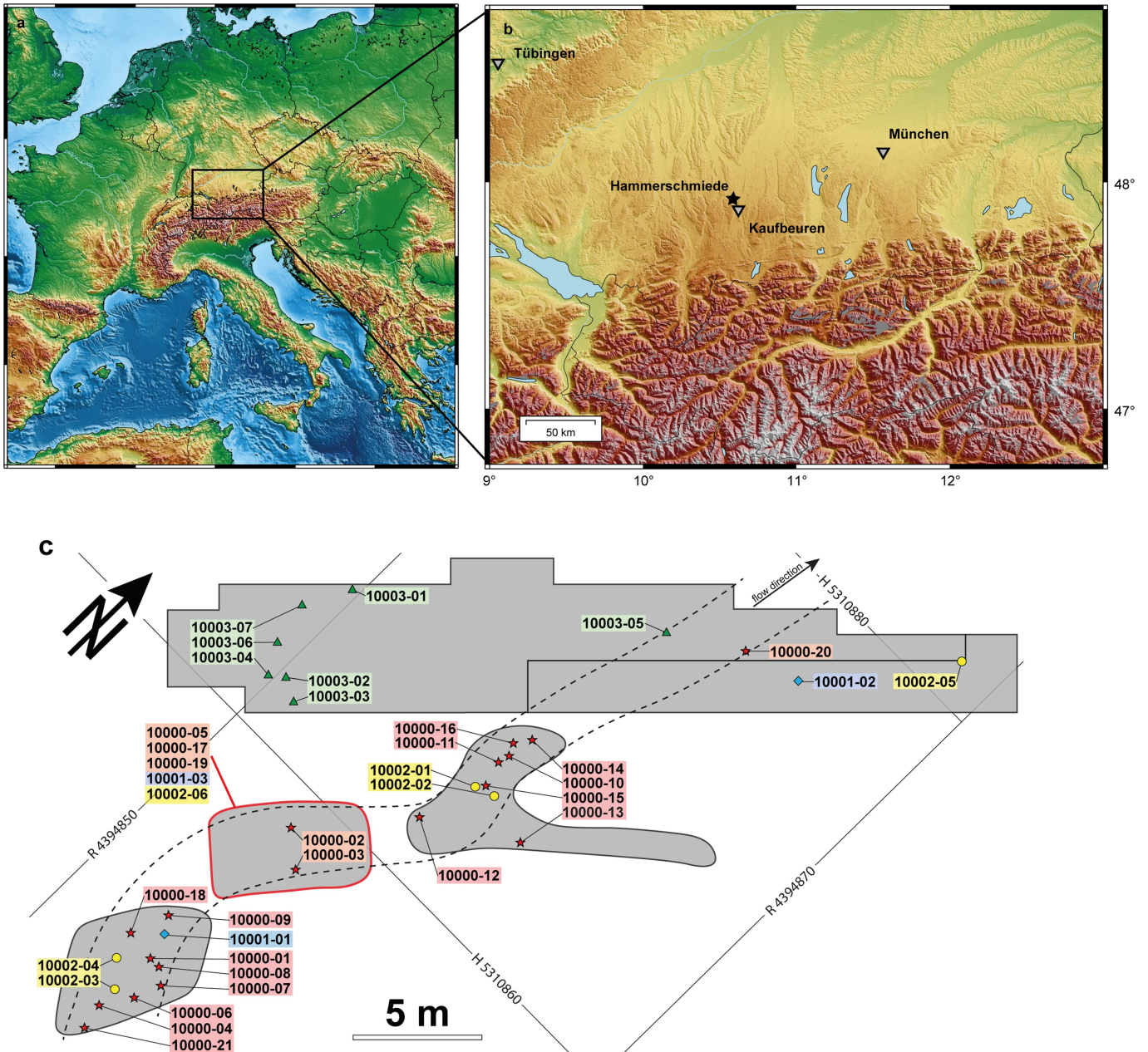
Additional information

Supplementary information is available for this paper at <https://doi.org/10.1038/s41586-019-1731-0>.

Correspondence and requests for materials should be addressed to M.B.

Peer review information Nature thanks Jeremy M. DeSilva, Tracy Kivell and Salvador Moyà-Solà for their contribution to the peer review of this work.

Reprints and permissions information is available at <http://www.nature.com/reprints>.



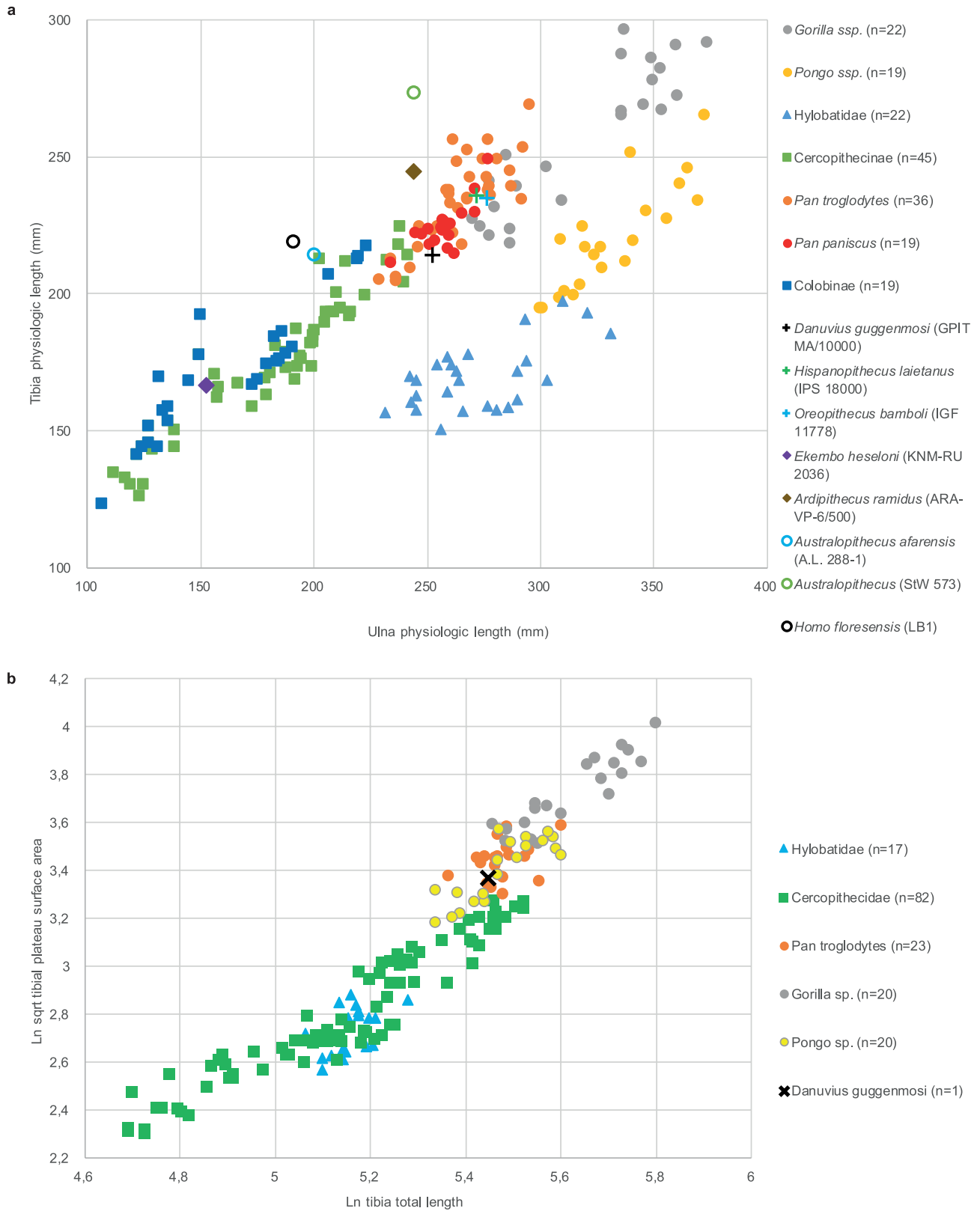
Extended Data Fig. 1 | Localization of Hammerschmiede locality and excavation plan with localized *D. guggenmosi* specimens. **a**, Topographical map of Europe. **b**, Magnification of the western part of the south German Molasse Basin (North Alpine Foreland Basin). The Hammerschmiede locality (47° 55' 37" N, 10° 35.5' E) is highlighted with a black star. Both maps were created using Generic Mapping Tools⁴⁷ and topographic datasets ETOPO1⁴⁸ and SRTM3⁴⁹. **c**, Excavation plan of the HAM 5 layer (the section has previously been published¹⁵) with excavated areas coloured in grey. Intermediate regions represent material lost due to clay mining. Dashed lines indicate the reconstructed thalweg course of the palaeochannel. Different colours and symbols indicate the individual context: holotype (GPIT/MA/10000) adult

male marked in red (stars), paratype (GPIT/MA/10001) female 1 in blue (diamonds), paratype (GPIT/MA/10002) juvenile individual in yellow (circles) and paratype (GPIT/MA/10003) female 2 in green (triangles). The red encircled sector indicates removed and stored sediments that were screen washed separately. This area was under threat of destruction from quarry activity. To avoid the complete loss of this sediment, approximately 25 tonnes were removed for remote processing. Two specimens were recovered in situ in this area. Five other specimens from this area were recovered during subsequent screen washing and cannot be more precisely localized. Coordinates correspond to Gauss-Krüger Zone 4 grid with easting (R) and northing (H) in metres.



Extended Data Fig. 2 | *D. guggenmosi*, dental and cranial specimens. **a**, Left maxilla with P³-M² (GPIT MA/10000-01) in lateral, anterior, medial (top), palatal, posterior, superior (bottom) views. **b**, Left mandible (GPIT MA/10000-02) in lateral, anterior, medial and occlusal views. **c**, Left upper central incisor (GPIT MA/10002-01) in labial, lingual and occlusal views. **d**, Right upper P³ fragment (GPIT MA/10000-05) in buccal, occlusal and mesial views. **e**, Left P³ (GPIT MA/10001-03) in buccal, occlusal and mesial views. **f**, Right upper M¹ (GPIT MA/10001-01) in occlusal, medial, distal and buccal views. **g**, Left lower P₃

(GPIT MA/10000-07) in medial, buccal, lingual and occlusal views. **h**, Left lower lateral incisor (GPIT MA/10003-5) in distal, mesial, lingual and labial views. **i**, Left lower central incisor (GPIT MA/10000-08) in distal, mesial and lingual views. **j**, Right lower P₃ (GPIT MA/10000-06) in mesial, distal, buccal and occlusal views. **k**, Right lower M₂ (GPIT MA/10000-03) in lingual, buccal (top), mesial, distal (bottom) and occlusal views. **l**, Right lower M₃ (GPIT MA/10000-04) in lingual, mesial (top), buccal, distal (bottom) and occlusal views. Scale bar, 10 mm.



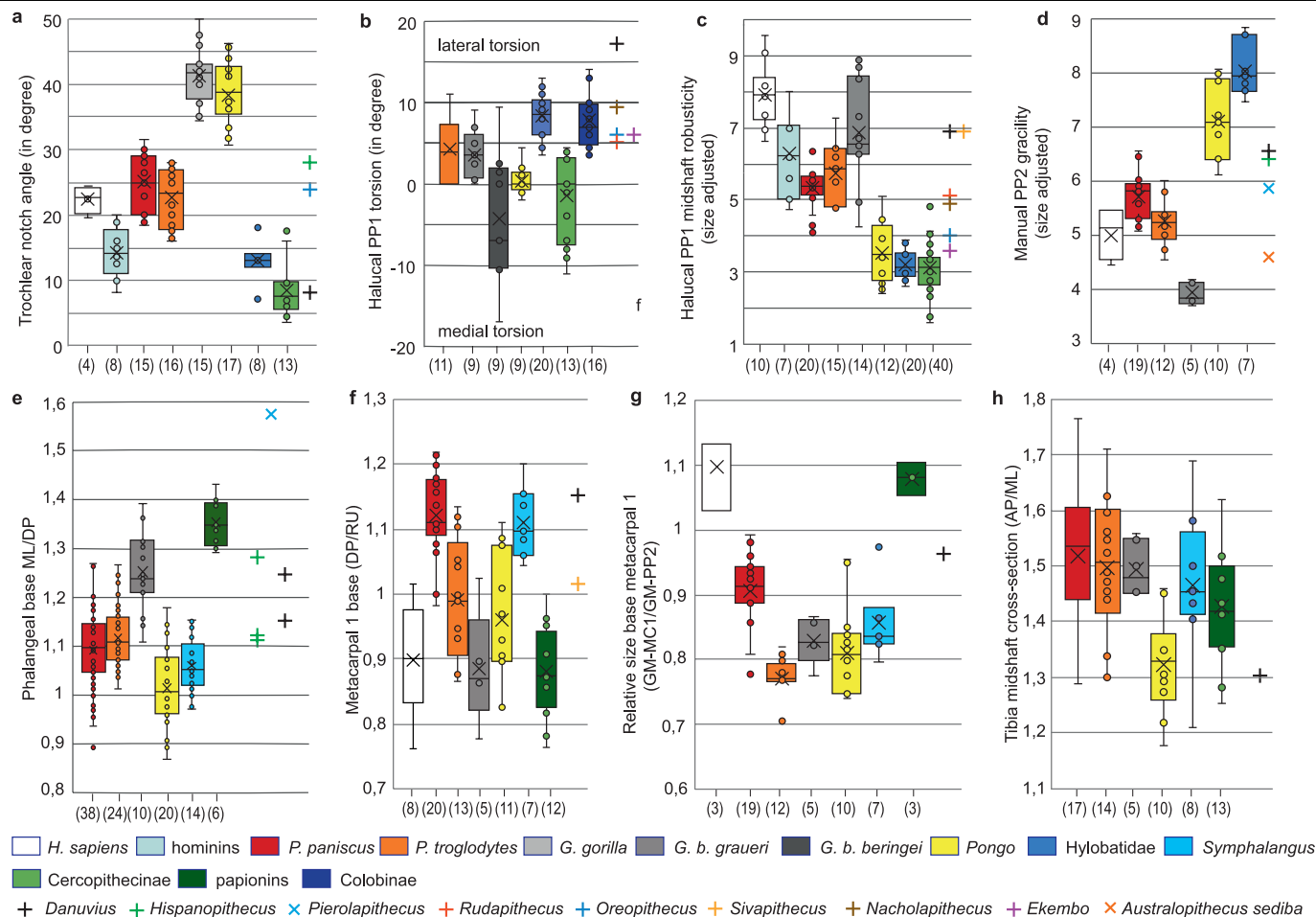
Extended Data Fig. 3 | Long-bone relationships and tibial plateau surface area. **a**, Relationships of physiologic lengths of tibia and ulna among extant and fossil catarrhines. **b**, Relationships of tibial plateau surface area (TPSA sensu³⁹, natural logarithm of square root) and tibial total length (natural logarithm)

among extant hominids, hylobatids and cercopithecids (comparative data from a previous study³⁹). The tibial plateau surface area of GPIT MA/10000-10 is 1,457 mm².



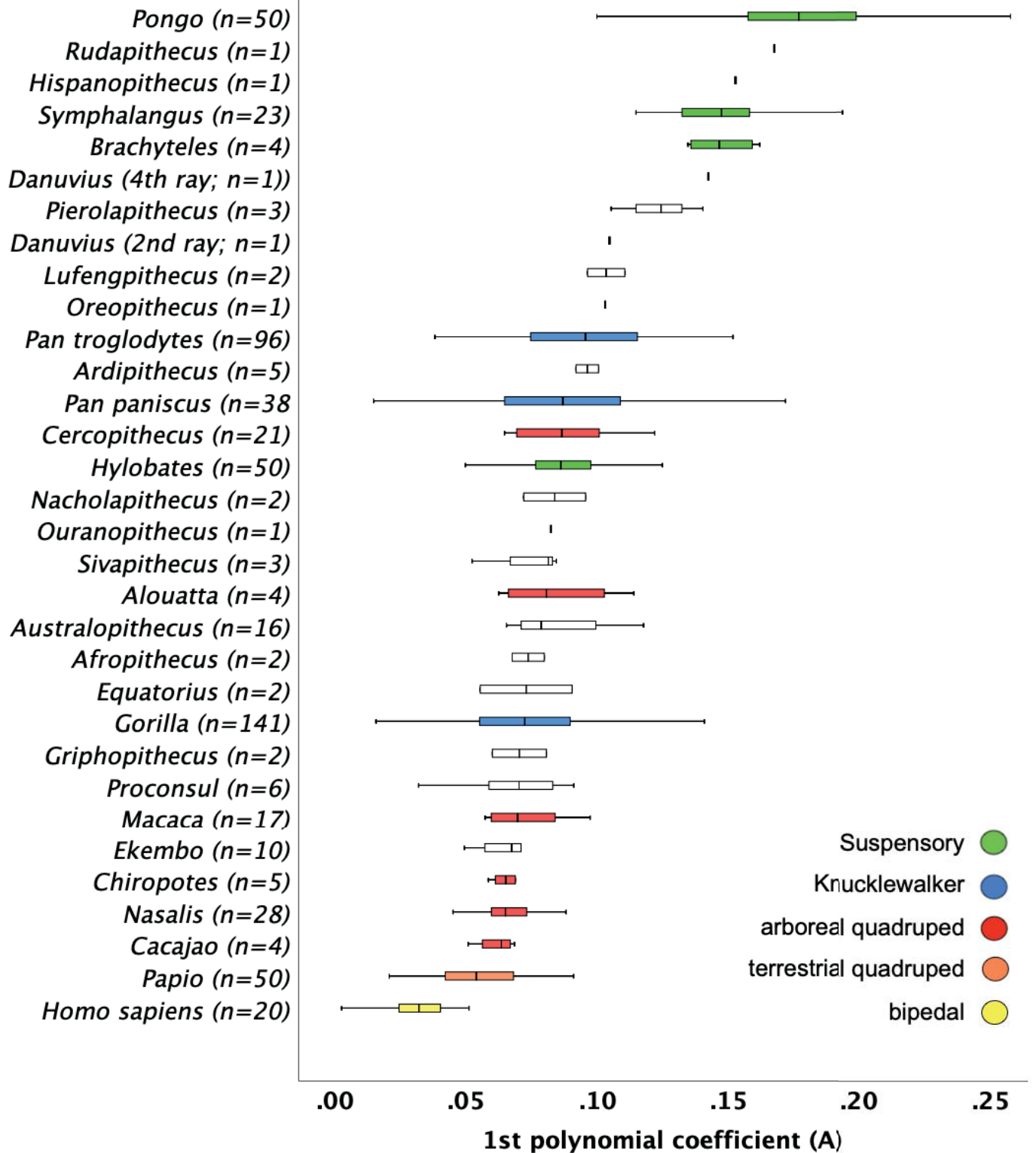
Extended Data Fig. 4 | *D. guggenmosi*, additional views of right ulna (GPIT MA/10000-10) and left tibia (GPIT MA/10000-15). a–d, Lateral (a), anteromedial (b) and posterior (c) views of the ulna and the reconstructed

olecranon in anterior view (d). e, f, Medial (e) and lateral (f) views of the tibia. Scale bar, 20 mm.



Extended Data Fig. 5 | Ulnar trochlear notch, phalangeal, metacarpal and tibial midshaft comparisons. **a**, Ulnar trochlear notch angle (for raw data, see Supplementary Table 9). **b**, Hallucal proximal phalanx (PP1) torsion (for measurement, see Methods; for raw data, see Supplementary Table 23). **c**, Size-adjusted hallucal proximal phalanx (PP1) midshaft robusticity (MLms \times DPms/GM in which MLms is the mediolateral width at midshaft, DPms is the dorsopalmar height at midshaft and GM is the geometric mean of the seven measurements: ML and DP at proximal, distal and midshaft, and total length; for raw data, see Supplementary Table 22). **d**, Size-adjusted second manual proximal phalanx (PP2) gracility (TL/GM in which TL is the total length and GM is the geometric mean of five measurements: ML and DP at distal and midshaft, and TL; five measurements are used to include *Pierolapithecus catalaunicus*, in which the proximal articulation is damaged⁵⁰; for raw data, see Supplementary

Table 11). **e**, Manual phalangeal base, ratio of mediolateral (ML) to dorsopalmar (DP) length (for raw data, see Supplementary Tables 11, 12). **f**, Manual metacarpal 1 base, ratio of dorsopalmar to radioulnar (RU) length (for raw data, see Supplementary Table 10). **g**, Relative size of manual metacarpal 1 base (geometric mean of dorsopalmar and radioulnar lengths) to proximal phalanx of ray 2 (geometric mean of seven measurements; for raw data, see Supplementary Tables 10, 11). **h**, Tibial cross-section at midshaft (ratio of anteroposterior and mediolateral width; for raw data see Supplementary Table 21). Sample sizes (n) of biologically independent animals are reported in parentheses below each box plot. All box plots show the centre line (median), box limits (upper and lower quartiles), crosses (arithmetic mean), whiskers (range) and individual values (circles).



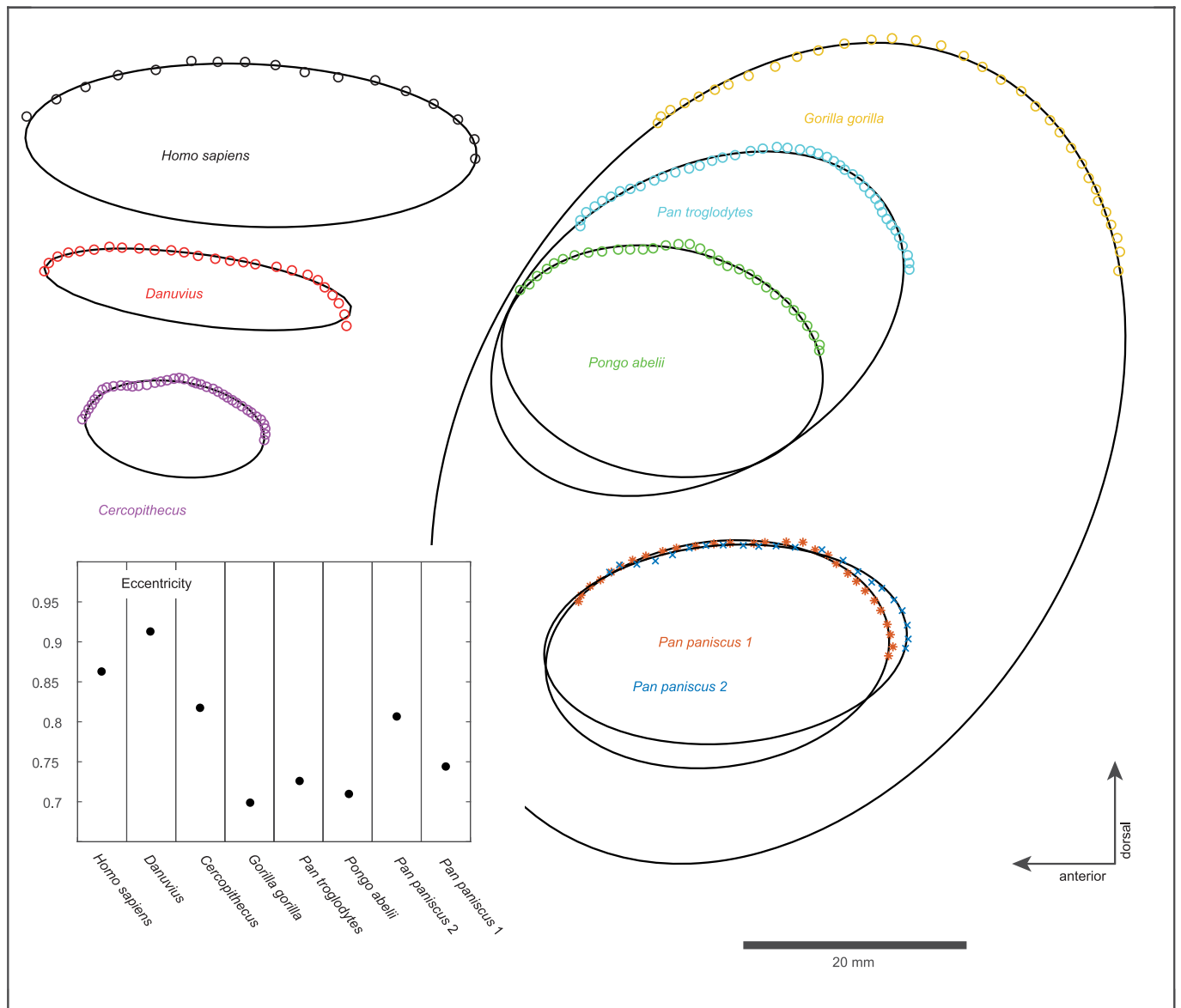
Extended Data Fig. 6 | Curvature manual proximal phalanges. Box plots of the first polynomial coefficient (A) of the second-order polynomial functional representing phalangeal shaft curvature. The box represents the interquartile range, which represents 50% of the sample values. The whiskers are lines that extend from the interquartile range box to the highest and lowest values,

excluding outliers. The line across the box indicates the median sample value for coefficient A. Extant primates are colour-coded according to locomotor adaptation. Taxa are arranged according to ascending median phalangeal shaft curvature. Sample sizes (*n*) of biologically independent animals are reported in parentheses after the species names.



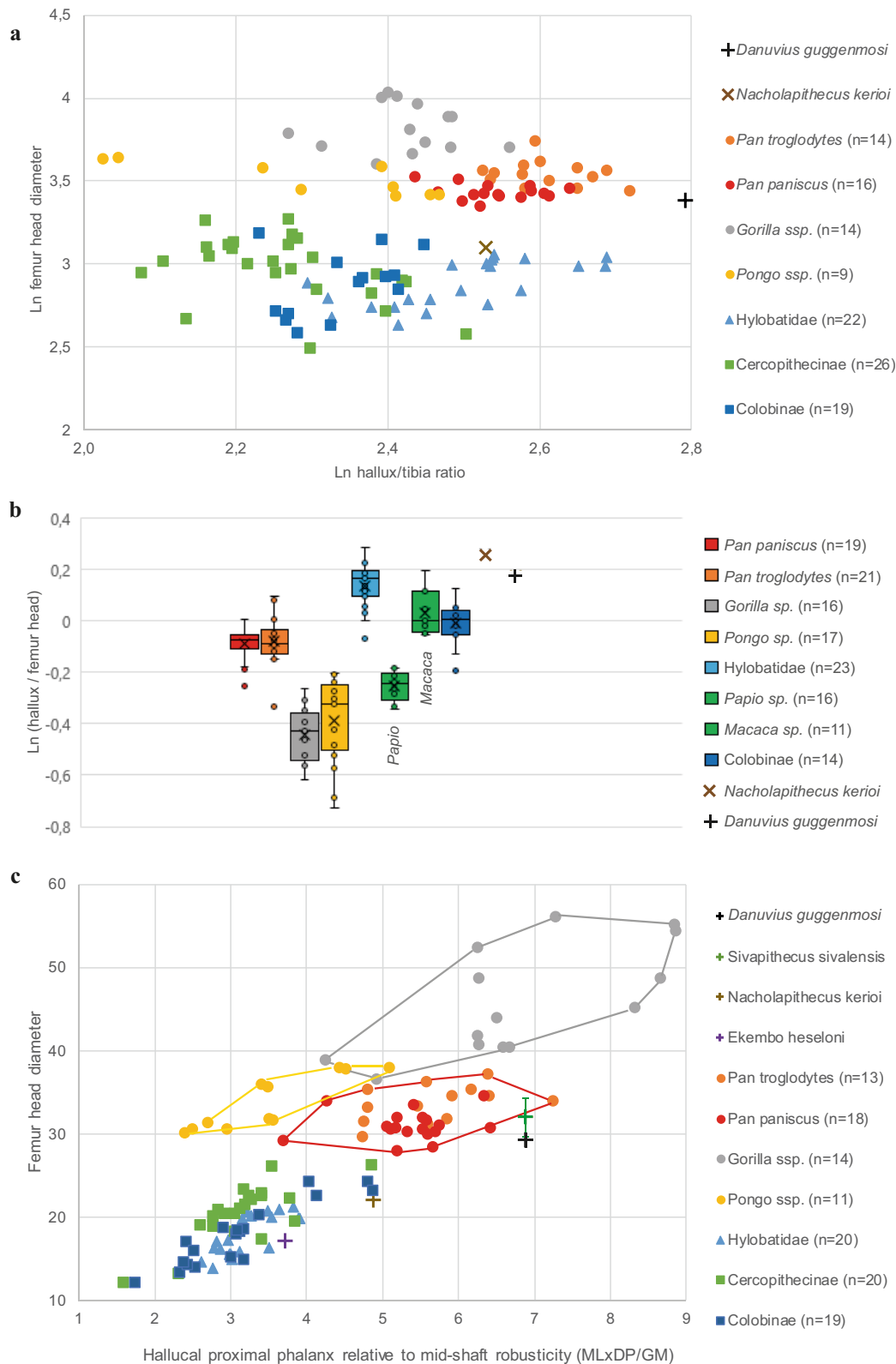
Extended Data Fig. 7 | *D. guggenmosi*, patella and femora. a. Right patella (GPIT MA/10000-12) in external and internal views. **b.** Right femur head (GPIT MA/10000-11) in medial, anterior, posterior (top), superior and lateral (bottom) views. **c.** Left femur head (GPIT MA/10001-02) in medial, posterior,

anterior (top), superior and lateral (bottom) views. **d.** Left femur, proximal half (GPIT MA/10003-01) in anterior (top) and posterior (bottom) views. Scale bar, 10 mm.



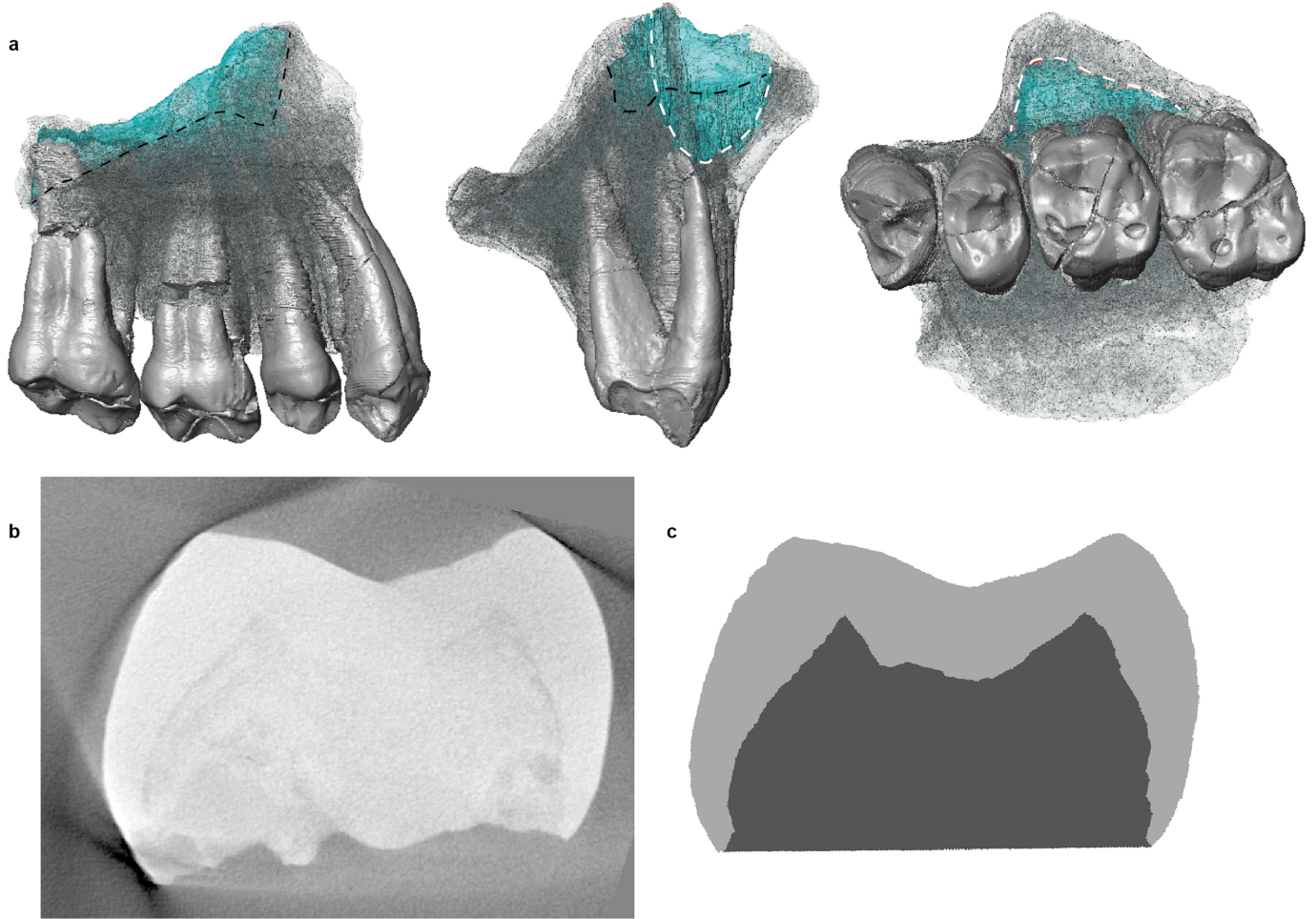
Extended Data Fig. 8 | Ellipse estimates of lateral tibial condyle. Best fit ellipses to digitalized portions of sagittal cross-sections through lateral tibial condyle of *D. guggenmosi* and extant catarrhines. Digitalized dots are shown in colour and best-fit ellipses in black. Orientation of ellipses follows the lateral condyle orientation (dorsal is up, anterior is left) at the same scale (scale bar,

20 mm). Inset shows calculated values of eccentricity for the obtained ellipses. Results indicate that both *Danuvius* and extant humans have a flat lateral tibial condyle (eccentricity >0.85), whereas great apes exhibit a convex lateral condyle (eccentricity <0.80) and *Cercopithecus* occupy an intermediate position.



Extended Data Fig. 9 | Hallux length and robusticity. a, Ratio (natural logarithm) of proximal hallucal phalanx total length to tibial physiologic length, relative to body mass (maximum femur head diameter). **b,** Box plots of hallux to femur head diameter ratios (natural logarithm). Box plots show the centre line (median), box limits (upper and lower quartiles), cross (arithmetic

mean), whiskers (range) and individual values (circles). **c,** Size-adjusted hallucal phalanx midshaft robusticity (for explanation, see Extended Data Fig. 8c), relative to femur head diameter. All sample sizes (*n*) of biologically independent animals are reported in parentheses after the species names. For raw data, see Supplementary Tables 7, 22.



Extended Data Fig. 10 | *D. guggenmosi*, maxillary sinus and enamel thickness. **a**, Left maxilla with three-dimensional rendering of molar roots and maxillary sinus (blue) in lingual (left), anterior (middle) and occlusal (right) views. Sinus runs deep between the posterobuccal and lingual roots of M^2 , rising anteriorly (dashed black line). Laterally the sinus extends deep into the

zygomatic root (dashed white line). **b, c**, Enamel thickness measured on right M_2 (GPIT/MA 10000-03). Computed tomography image of the cross-section at distal sectional plane (**b**) and graphical conversion (**c**; grey, enamel; dark grey; dentine).

Reporting Summary

Nature Research wishes to improve the reproducibility of the work that we publish. This form provides structure for consistency and transparency in reporting. For further information on Nature Research policies, see [Authors & Referees](#) and the [Editorial Policy Checklist](#).

Statistical parameters

When statistical analyses are reported, confirm that the following items are present in the relevant location (e.g. figure legend, table legend, main text, or Methods section).

n/a | Confirmed

- The exact sample size (n) for each experimental group/condition, given as a discrete number and unit of measurement
- An indication of whether measurements were taken from distinct samples or whether the same sample was measured repeatedly
- The statistical test(s) used AND whether they are one- or two-sided
Only common tests should be described solely by name; describe more complex techniques in the Methods section.
- A description of all covariates tested
- A description of any assumptions or corrections, such as tests of normality and adjustment for multiple comparisons
- A full description of the statistics including central tendency (e.g. means) or other basic estimates (e.g. regression coefficient) AND variation (e.g. standard deviation) or associated estimates of uncertainty (e.g. confidence intervals)
- For null hypothesis testing, the test statistic (e.g. F , t , r) with confidence intervals, effect sizes, degrees of freedom and P value noted
Give P values as exact values whenever suitable.
- For Bayesian analysis, information on the choice of priors and Markov chain Monte Carlo settings
- For hierarchical and complex designs, identification of the appropriate level for tests and full reporting of outcomes
- Estimates of effect sizes (e.g. Cohen's d , Pearson's r), indicating how they were calculated
- Clearly defined error bars
State explicitly what error bars represent (e.g. SD, SE, CI)

Our web collection on [statistics for biologists](#) may be useful.

Software and code

Policy information about [availability of computer code](#)

Data collection

Data was collected on the original specimen using a phoenix v|tome|x s CT scanner at GeoZentrum Nordbayern (Friedrich-Alexander Universität Erlangen-Nürnberg, Germany) and a YXLON FF35 CT scanner at YXLON Inspection Service facility (Heidelberg / Germany). Comparative data of extant species were collected by using an Artec Space Spider surface scanner and Artec Studio software (versions 11-14).

Data analysis

For the micro CT-scan data analysis, we used Avizo 9.0 (ThermoFisher Scientific) and Geomagic Wrap 2017 (3D Systems Software) for the virtual reconstruction of longbones. 3D-prints were generated with Z-Suite 2.11 and printed on a Zortrax M200 FDM printer. Lateral tibia ellipse estimates we obtained using the Matlab function "EllipseDirectFit" of Nikolai Chernov available from mathworks.com

For manuscripts utilizing custom algorithms or software that are central to the research but not yet described in published literature, software must be made available to editors/reviewers upon request. We strongly encourage code deposition in a community repository (e.g. GitHub). See the Nature Research [guidelines for submitting code & software](#) for further information.

Data

Policy information about [availability of data](#)

All manuscripts must include a [data availability statement](#). This statement should provide the following information, where applicable:

- Accession codes, unique identifiers, or web links for publicly available datasets
- A list of figures that have associated raw data
- A description of any restrictions on data availability

All data generated or analysed during this study are included in the published article (and its supplementary information files). The CT-scans analysed during the current study are available from the corresponding author on reasonable request.

Field-specific reporting

Please select the best fit for your research. If you are not sure, read the appropriate sections before making your selection.

Life sciences Behavioural & social sciences Ecological, evolutionary & environmental sciences

For a reference copy of the document with all sections, see [nature.com/authors/policies/ReportingSummary-flat.pdf](https://www.nature.com/authors/policies/ReportingSummary-flat.pdf)

Ecological, evolutionary & environmental sciences study design

All studies must disclose on these points even when the disclosure is negative.

Study description	Morphologic description and functional interpretation of fossil hominid specimens.
Research sample	The research sample consists of 36 original fossil hominid bones/teeth from Hammerschmiede. The extant primates samples for skeletal comparison consists of about 350 adult and non-captive individuals of cercopithecids and hominids of both sexes.
Sampling strategy	No sample size calculation was performed. The sample size of fossils is limited by availability. The size of extant comparative samples (primates) varies between 10 and 60 individuals, which is a normal size in primatological anatomic comparisons.
Data collection	Data from the original fossil specimens were collected by M.B, D.R.B., N.S. and J.F. Micro-CT and surface scan data processing and collection was conducted by J.F. and A.T., in collaboration with A.S.D., U.K., T.L. and J.P.
Timing and spatial scale	Data collection started in spring 2018, followed by comparative data collection from summer 2018 to summer 2019.
Data exclusions	No data was excluded from the analysis.
Reproducibility	not applicable
Randomization	not applicable
Blinding	not applicable
Did the study involve field work?	<input type="checkbox"/> Yes <input type="checkbox"/> No

Field work, collection and transport

Field conditions	not applicable for palaeontological excavations
Location	Hammerschmiede, Allgäu, Bavaria, southern Germany;), coordinates N 47° 55' 38.5", E 10° 35.5'; fluvial channel of level HAM 5 at stratigraphic meter 12 in the local section, 685 m above sea level
Access and import/export	According to German (Bavarian) law no permissions needed for palaeontological excavations. Permission from the land owner have been obtained.
Disturbance	No disturbance (active mining pit)

Reporting for specific materials, systems and methods

Materials & experimental systems

n/a	Involvement	Included
<input checked="" type="checkbox"/>	<input type="checkbox"/>	Unique biological materials
<input checked="" type="checkbox"/>	<input type="checkbox"/>	Antibodies
<input checked="" type="checkbox"/>	<input type="checkbox"/>	Eukaryotic cell lines
<input type="checkbox"/>	<input checked="" type="checkbox"/>	Palaeontology
<input checked="" type="checkbox"/>	<input type="checkbox"/>	Animals and other organisms
<input checked="" type="checkbox"/>	<input type="checkbox"/>	Human research participants

Methods

n/a	Involvement	Included
<input checked="" type="checkbox"/>	<input type="checkbox"/>	ChIP-seq
<input checked="" type="checkbox"/>	<input type="checkbox"/>	Flow cytometry
<input checked="" type="checkbox"/>	<input type="checkbox"/>	MRI-based neuroimaging

Palaeontology

Specimen provenance	See above: According to German (Bavarian) law no permissions needed for palaeontological excavations. Non-formal permission from the land owner have been obtained.
Specimen deposition	All Hammerschmiede fossils are stored in the paleontological collection of the University of Tübingen (acronym GPIT), a research infrastructure of the Senckenberg Institute for Human Evolution and Palaeoenvironment (SHEP) Tübingen.
Dating methods	No new dates are provided.
<input checked="" type="checkbox"/> Tick this box to confirm that the raw and calibrated dates are available in the paper or in Supplementary Information.	